Measurements of Diffusion Resonances for the Atom Optics Quantum Kicked Rotor

M.E.K. Williams, M.P. Sadgrove, A.J. Daley, R.N.C. Gray, S.M Tan, A.S. Parkins, and R. Leonhardt
Department of Physics, University of Auckland, Private Bag 92019, Auckland, New Zealand

N. Christensen
Physics and Astronomy, Carleton College, Northfield, MN 55057

We present experimental observations of diffusion resonances for the quantum kicked rotor with weak decoherence. Cold caesium atoms are subject to a pulsed standing wave of near-resonant light, with spontaneous emission providing environmental coupling. The mean energy as a function of the pulse period is determined during the late-time diffusion period for a constant probability of spontaneous emission. Structure in the late-time energy is seen to increase with physical kicking strength. The observed structure is related to Shepelyansky's predictions of the initial quantum diffusion rates. Additional results of diffusion rates as a function of the effective Planck's constant are given, showing non-trivial behaviour in the quantum-to-classical transition regime.

PACS numbers: 05.45.Mt, 03.65.Yt, 32.80.Lg, 42.50.Lc

I. INTRODUCTION

The atom-optics realization of the kicked rotor has enabled the experimental study of the transition between quantum and classical behaviour for this fundamental non-linear system. For example, the effects of decoherence, the mechanism whereby quantum interference effects are destroyed via environmental coupling [1], have been studied in the quantum system. More classical behaviour is observed when decoherence is added, either by spontaneous emission events [2, 3, 4] or amplitude noise [5, 6]. However, recent theoretical studies have concentrated on what is perhaps a more direct approach of studying the quantum-to-classical transition - varying the action of the system and thereby the effective Planck's constant, i.e., increasing the action to investigate the limit in which '$\hbar$'$\to 0$ [7, 8]. Of particular interest in these studies is the behaviour found for intermediate values of '$\hbar$', where pronounced diffusion "resonances" are predicted to exist.

In this paper we present experimental observations of such diffusion resonances, the structure of which can be traced to a scaling formula for the initial quantum diffusion rate derived by Shepelyansky [9] and confirmed experimentally by Klappauf *et al.* [10]. An effective "locking in" [7] of the initial rates due to decoherence leads to the same structure being observable in late-time energies and diffusion rates.

The system and model that we study is presented in Sec. II, while the analysis of classical and quantum momentum diffusion in this system is discussed in Sec. III. Our experimental set-up is described in Sev. IV, and the results (experimental, quantum and classical calculations) are presented in Sec. V. The conclusion is in Sec. VI.

II. SYSTEM AND MODEL

For our system we use a laser-cooled cloud of caesium atoms of initial temperature ≈ 20 μK interacting with a standing wave of off-resonant laser light. The laser is pulsed with period T and pulse profile $f(t)$. If the laser-atom detuning is large the internal atomic dynamics can be eliminated and the motion of the caesium atoms is described by the single particle Hamiltonian [11]

$$\hat{H} = \frac{\hat{p}^2}{2m} - \frac{\hbar\Omega_{\rm eff}}{8}\cos(2k_{\rm L}\hat{x})\sum_{n=0}^{N} f(t-nT), \qquad (1)$$

where $\hat{x}$ and $\hat{p}$ are operators representing the atomic position and momentum, respectively, and $k_{\rm L}$ is the wave number of the laser light. The effective potential strength, $\Omega_{\rm eff} = \Omega^2(s_{45}/\delta_{45}+s_{44}/\delta_{44}+s_{43}/\delta_{43})$, accounts for dipole transitions between different combinations of hyperfine levels in the caesium atoms ($6S_{1/2}(F=4) \to 6P_{3/2}(F'=5)$), where δ_{ij} are the corresponding detunings between laser and atomic transiton frequencies, and $\Omega/2$ is the resonant single-beam Rabi frequency. If we assume equal populations of atoms in all ground state Zeeman sublevels, then $s_{45} = \frac{11}{27}$, $s_{44} = \frac{7}{36}$, and $s_{43} = \frac{7}{108}$. It is useful to rewrite this Hamiltonian in appropriate dimensionless units as

$$\hat{\mathcal{H}} = \frac{\hat{\rho}^2}{2} - k\cos(\hat{\phi})\sum_{n=0}^{\infty} f(\tau-n), \qquad (2)$$

which is the usual expression for the Hamiltonian of the standard kicked rotor system. In these units - which will be referred to as "scaled units" - the position operator is defined by $\hat{\phi} = 2k_{\rm L}\hat{x}$, the momentum operator is $\hat{\rho} = 2k_{\rm L}T\hat{p}/m$, time is rescaled as $\tau = t/T$, and our new Hamiltonian is related to Eq. (1) by $\hat{\mathcal{H}} = (4k_{\rm L}^2T^2/m)\hat{H}$. The classical stochasticity parameter is given by $\kappa = \Omega_{\rm eff}\omega_{\rm r}T\tau_p$, where $\tau_{\rm p}$ is the pulse length in unscaled time and $\omega_{\rm r} = \hbar k_{\rm L}^2/2m$. In our experiments, $f(\tau)$ is a good approximation to a square pulse,

i.e., $f(\tau) = 1$ for $0 < \tau < \alpha$, where $\alpha = \tau_{\rm p}/T$. Note that $k = \kappa/\alpha$.

In scaled units we have $[\hat{\phi}, \hat{\rho}] = i\bar{k}$, with $\bar{k} = 8\omega_{\rm r}T$, so that the quantum behaviour of our system is reflected by an effective Planck's constant, $\bar{k}$, which increases as we increase the pulse period T. This reflects our ability to change the total action in the system, and hence how classically our system behaves (for larger $\bar{k}$ values the quantum nature of the system should be more apparent). Note that the effective Planck's constant is proportional to the ratio of the total classical action of the system to $\hbar$.

The natural experimental unit for momentum is that of two photon recoils, $2\hbar k_{\rm L}$, and $p/(2\hbar k_{\rm L})$ will henceforth be referred to as the momentum in experimental units. We note the relationship $\rho/\bar{k} = p/(2\hbar k_{\rm L})$ and also define the quantity $\phi_{\rm d} = \kappa/\bar{k} = \Omega_{\rm eff}\tau_p/8$ as a dimensionless measure of the physical kicking strength. Experimentally, it is easier to hold this quantity constant, rather than κ, as T is varied as a constant value of $\phi_{\rm d}$ corresponds to constant pulse duration, standing wave detuning and power (whereas κ is proportional to T).

Our system is coupled to its environment via atomic spontaneous emission events, which occur when the caesium atoms absorb photons from the standing wave [2] and then spontaneously re-emit the photons in random directions. We characterise the level of this decoherence by the probability of spontaneous emission per atom per kick, η. Given the large detuning, i.e., $\Omega_{\rm eff}/\delta \ll 1$, this process may be modeled by the following master equation for the density operator $\hat{w}$ of the system [3],

$$\begin{aligned}\dot{\hat{w}} \;=\; & -i[\hat{\mathcal{H}}, \hat{w}] - \frac{\eta}{\alpha}\sum_{n=0}^{N} f(\tau - n)[\cos^2(\hat{\phi}/2), \hat{w}]_+ \\ & +2\frac{\eta}{\alpha}\sum_{n=1}^{N} f(\tau - n)\int_{-1}^{1} du N(u) e^{iu\hat{\phi}/2} \\ & \times \cos(\hat{\phi}/2)\hat{w}\cos(\hat{\phi}/2)e^{-iu\hat{\phi}/2}, \end{aligned} \tag{3}$$

where $N(u)$ is the distribution of recoil momenta projected onto the axis of the standing wave, and $[.,.]_+$ denotes an anti-commutator. Simulations of Eq. (3) are used for comparisons with the experiment.

III. MOMENTUM DIFFUSION

We measure the total kinetic energy of the cloud after N kicks, which depends on the initial energy of the cloud plus the increase in the kinetic energy resulting from the kicks. The amount of increase for kick number n is the momentum diffusion rate, given by $2D(n) = \langle\hat{\rho}_{n+1}^2\rangle - \langle\hat{\rho}_n^2\rangle$, where we denote $\hat{\rho}_0 = \hat{\rho}(t' = 0)$, $\hat{\rho}_1 = \hat{\rho}(t' = 1)$, etc.. For a kicked rotor system with a sufficiently broad initial momentum distribution, we expect $D(0) = D(1) = \kappa^2/4$. The system then passes through an initial quantum diffusion period lasting typically for around 5 kicks [8], with a diffusion rate approximated by the result of Shepelyansky (under the conditions $\bar{k} \geq 1$ and $\kappa \gg \bar{k}$) [9],

$$D_{\rm q} = \frac{\kappa^2}{2}\left(\frac{1}{2} - J_2(K_{\rm q}) - J_1^2(K_{\rm q}) + J_2^2(K_{\rm q}) + J_3^2(K_{\rm q})\right), \tag{4}$$

where $K_{\rm q} = 2\kappa\sin(\bar{k}/2)/\bar{k}$. Note that the classical diffusion rate is also given by Eq. (4), but with $K_{\rm q} \to \kappa$ (i.e., $\bar{k} \to 0$).

Without decoherence, the system generally settles into a localised state [12], but the loss of phase coherence produced by the addition of spontaneous emission causes the system to settle instead into a final steady state diffusion regime, with a late time diffusion rate which may be approximated by the formula [2, 8, 12]

$$D_\infty = \sum_{n=0}^{\infty} \eta(1-\eta)^n D_0(n), \tag{5}$$

where $D_0(n)$ is the diffusion rate at the nth kick for a kicked rotor *without* decoherence. Essentially, this formula assumes that dynamical correlations over particular time intervals which give rise to the late time diffusion rates are suppressed by a factor equal to the probability that a spontaneous emission occurs within that time interval. The correlations taken over a set number of kicks give rise to the diffusion rates seen in the kicked rotor without decoherence after that number of kicks, which leads to the late time diffusion rate being an appropriate weighted average over the diffusion rates as the kicked rotor "settles down" [8]. Thus, the diffusion rates in the first few kicks are essentially "locked in" by the spontaneous emission events, and we observe similar structure in the late time diffusion rates as we vary T to that observed in the initial quantum diffusion rates.

The structure we observe in the initial quantum diffusion rates as we vary T for constant $\phi_{\rm d}$ with diffusion rates measured in experimental units is particularly interesting. We can express Shepelyansky's formula in this regime as

$$D'_{\rm q} = \frac{(\phi_d)^2}{2}\left(\frac{1}{2} - J_2(K'_{\rm q}) - J_1^2(K'_{\rm q}) + J_2^2(K'_{\rm q}) + J_3^2(K'_{\rm q})\right), \tag{6}$$

with $K'_{\rm q} = 2\phi_{\rm d}\sin(4\omega_{\rm r}T)$. We then see that any structure in the diffusion rates is periodic in T with period $2\pi/8\omega_{\rm r}$ (In fact, from Eq. (5) this is also true for the late time diffusion rates). We also see that the form of the structure depends solely on the value of $\phi_{\rm d}$. Fig. 1 shows the initial quantum diffusion rate as a function of pulse period for varying values of $\phi_{\rm d}$. We see the regular feature of a peak near the quantum resonance at $\bar{k} = 2\pi/8\omega_{\rm r}$ ($T = 60.4$ μs), and we see increasing numbers of enhanced diffusion peaks or resonances as we increase the value of $\phi_{\rm d}$.

The classical diffusion rate can be similarly found in this regime to be

$$D'_{\rm cl} = \frac{(\phi_d)^2}{2}\left(\frac{1}{2} - J_2(\kappa) - J_1^2(\kappa) + J_2^2(\kappa) + J_3^2(\kappa)\right), \tag{7}$$

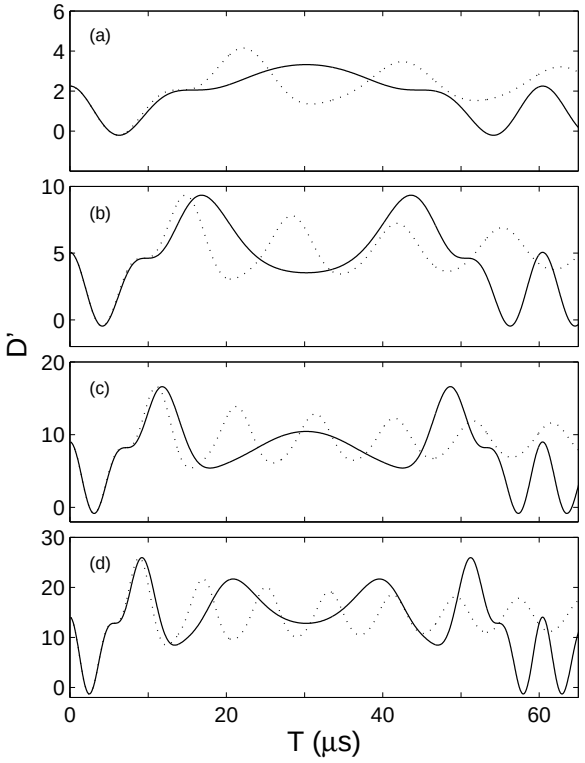

FIG. 1: Theoretical initial momentum diffusion rates in the quantum case (solid line), $D'_{\rm q}$ as given by Eq. (6), and the classical case (dotted line), $D'_{\rm cl}$ in Eq. (7), in experimental units of as a function of T for (a) $\phi_{\rm d} = 3$, (b) $\phi_{\rm d} = 4.5$, (c) $\phi_{\rm d} = 6$ and (d) $\phi_{\rm d} = 7.5$. The quantum resonance is seen in the quantum diffusion rate at $T = 60.4$ μs.

with $\kappa = 8\omega_{\rm r}T\phi_{\rm d}$. The second set of curves in Fig. 1 shows the classical rate for various $\phi_{\rm d}$. These rates oscillate around the quasilinear value which in these units is $(\phi_{\rm d})^2/4$, with the oscillations increasing in frequency with $\phi_{\rm d}$. For any given $\phi_{\rm d}$ however, the structure in the classical diffusion rate is markedly different to that in the initial quantum rate.

In the experiment, late-time energies were measured and not initial diffusion rates. However, the diffusion resonances discussed above are still observable. The existence of the same structures in the late time diffusion rates (in the presence of decoherence) as those in the initial quantum rates has been verified using the simulations described later in this paper. An approximate formula for the energy after N kicks can be found by summing the diffusion rate at each kick, that is

$$E'(N) = \frac{\langle\left(\frac{p}{2\hbar k_{\rm L}}\right)^2\rangle}{2} = \sum_{n=0}^{N-1} D'(n,T). \qquad (8)$$

Therefore, with the initial and final diffusion rates both displaying these structures, it follows that the energy at the Nth kick should also display them.

IV. EXPERIMENT

The experimental setup used was much the same as that used previously in our quantum chaos investigations [2, 13], with a few modifications. A standard six-beam magneto-optical trap was used to trap and cool approximately 10^5 caesium atoms. The trapping laser frequency was set about 10 MHz to the red of the $6S_{1/2}(F = 4) \rightarrow 6P_{3/2}(F' = 5)$ transition. A second (repump) laser was locked to the $6S_{1/2}(F = 3) \rightarrow 6P_{3/2}(F' = 4)$ transition to return those atoms lost to the $F = 3$ ground state to the trapping cycle. After a 20 ms cooling phase prior to kicking, the cloud had a temperature of approximately 20 μK and a width of $\sigma_{\rm cloud} \sim 270$ μm in its position distribution. Kicking of the cloud occurred for up to 2 ms during the 10 ms free expansion phase, at the completion of which the cloud was "frozen" in space by the molasses beams and imaged. The repumping beam was left on during the kicking to prevent loss of atoms to the $F = 3$ ground state. The resultant heating effect was negligible for our experiments.

A third laser was used to create a pulsed optical standing wave across the cloud. A relatively high power laser diode was injection locked with a frequency stabilised external cavity laser, giving a beam of up to 22 mW CW power. For fast switching the beam passed through a 80 MHz Acousto-Optic Modulator (AOM) in front of a single mode polarisation preserving optical fibre. Temporal modulation was provided via the RF supply to the AOM, generating pulse shapes very close to rectangular. The linearly polarised beam was then collimated giving a beam radius at the cloud of $2\sigma_{\rm beam} = 1$ mm. Finally, to create a standing wave the beam was retroreflected by a mirror outside the vacuum cell. The atoms experienced a range of optical potential depths as the cloud's width was comparable in size to that of the laser beam. If $\phi_{\rm d,max}$ is the kicking strength along the beam axis then the mean value was found to be $\phi_{\rm d,mean} \approx 0.77\phi_{\rm d,max}$ with a standard deviation of 18%. In the following, $\phi_{\rm d}$ will always refer to $\phi_{\rm d,mean}$. The detuning of the kicking beam to the blue of the $F = 4 \rightarrow F' = 5$ transition was monitored as a beat frequency of the superposition of the trapping and kicking beams. Both the beam detuning and intensity were chosen to give a desired $\phi_{\rm d}$ while maintaining a constant spontaneous emission rate. The range of $\phi_{\rm d}$ examined in this way was from $\phi_{\rm d} = 3.3$ to 6.6. Taking reflection losses at the cell windows into account, over this $\phi_{\rm d}$ range the Rabi frequency varied from $\Omega/2\pi = 34 - 76$ MHz with corresponding detunings of $\delta_{45}/2\pi = 315 - 740$ MHz, thus $\delta >> \Gamma, \Omega$ was satisfied for all $\phi_{\rm d}$ values considered.

For a chosen $\phi_{\rm d}$ the pulse length was held constant ($\tau_{\rm p} = 520$ ns), while the pulse period was varied from 2.5 μs to just above the quantum resonance at $T \approx 60$ μs. Thirty kicks were delivered to the cloud for each pulse period. The expanded cloud images were averaged over the dimension perpendicular to the kicking beam to yield the momentum distributions of the kicked cloud.

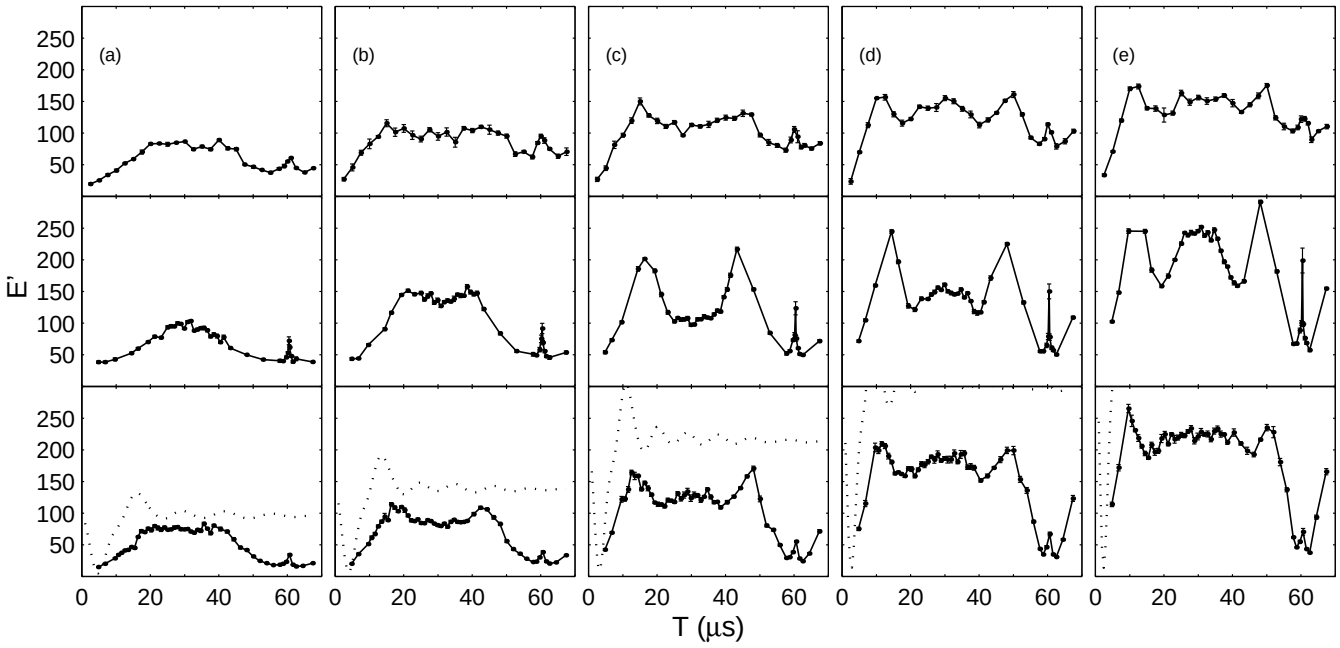

FIG. 2: Experimental results (top) and the corresponding quantum simulations with fixed $\phi_{\rm d}$ (middle) for the energy, E', after 30 kicks as a function of pulse period with $\tau_{\rm p} = 520$ ns, $\eta = 0.0125$ and for (a) $\phi_{\rm d} = 3.3$, (b) $\phi_{\rm d} = 4.0$, (c) $\phi_{\rm d} = 5.0$, (d) $\phi_{\rm d} = 5.9$ and (e) $\phi_{\rm d} = 6.6$. Additional quantum simulations (bottom, solid line) take into account the spread in physical kicking strength $\phi_{\rm d}$ as do the analytical classical results (bottom, dotted line). The energies are in experimental units and error bars for the results and simulations are shown but are very small.

From each distribution the mean energy $E = \langle p^2 \rangle/2$ was calculated. High momenta have a large effect on these energy values and as this was where the signal dropped for the higher energy kicked clouds, much care was taken to reduce the effects of noise. For an experimental run involving a single $\phi_{\rm d}$ value, the subtracted background was an average from just before and after the run. Any slight fluctuations in background level were accounted for by defining the zero level for each momentum distribution via an image taken just before commencement of the kicking sequence, omitting the small cloud. The signal-to-noise ratio was on average about 100:1 and for each value of T the momentum distribution was measured 5 times. Long term fluctuations in the kicking beam power after the fibre were caused by the transmission of the Fabry-Perot etalon set up between the fibre ends changing with time. To minimise the effects of this problem one fibre end was angle cleaved and the beam power was checked and readjusted several times throughout a run. These measures reduced the fluctuations in $\phi_{\rm d}$ from this source to $\sim 1\%$.

V. EXPERIMENTAL RESULTS

A. Varying T while keeping $\phi_{\rm d}$ constant

We have compared our results with numerical simulations of Eq.(3). The simulations are performed using the method of quantum trajectories, as in Ref. [8]. The simulations reflect a system with an initial Gaussian distribution in momenta of width $\sigma_\rho/\bar{k} = \sigma_p/2\hbar k_l = 4$ (this corresponds to a cloud of temperature $\approx 20\mu K$). They also take into account the effects of finite pulse widths, spontaneous emission noise, and small amplitude fluctuations in the kicking strength.

The results of both experiments and simulations giving the mean energy as a function of T for various values of $\phi_{\rm d}$ are given in Fig. (2). Firstly, the quantum resonance at $T \approx 60$ μs is seen to be present for all $\phi_{\rm d}$ values. Secondly, while a single broad peak similar to that seen by d'Arcy *et al.* [14] is found for $\phi_{\rm d} = 3.3$, for larger $\phi_{\rm d}$ values more complicated structure is observed. The peak splits and diverges, whereupon a second peak rises. The structure mirrors that in the initial quantum diffusion rate as given by Shepelyansky's result in Eq. (6) and shown in Fig. 1. For $\phi_{\rm d} = 3.3$ there is particularly good agreement between experiment and theory in peak height and structure. For higher $\phi_{\rm d}$ there is still good agreement in the position of the peaks, but discrepancies between the "peak-to-valley" energy differences for theory and experiment are apparent which are not accounted for by experimental error. Also, the broadness of the overall structure is greater in the experimental results than in the simulations especially for lower $\phi_{\rm d}$ values. There are a number of effects that can account for these discrepancies, which will be discussed below. However, we still see a clear correspondence between the

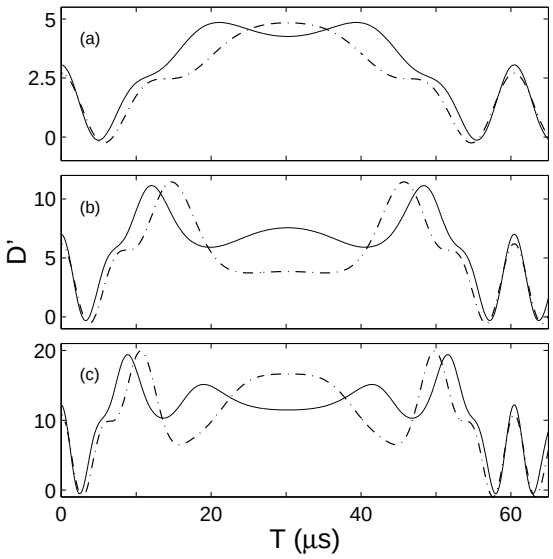

FIG. 3: Initial momentum diffusion rates, D', with constant $\phi_{\rm d}$ (dash-dotted line) and the experimental spread in $\phi_{\rm d}$ (solid line) in experimental units as a function of T for (a) $\phi_{\rm d} = 3.3$, (b) $\phi_{\rm d} = 5.0$ and (c) $\phi_{\rm d} = 6.6$.

resonance structure predicted via the simulations and observed experimentally, which are also clearly related to resonances predicted by Shepelyansky's result.

One source of discrepancy between our experimental results and the simulations shown in the middle row of Fig. (2) is the fact that the kick strength is not the same for all atoms. Firstly, there is a spread in physical kicking strengths due to the finite width of the kicking beam, which results in atoms at different radial positions across the beam interacting with laser fields of different intensity. The simulations of the middle row, however, assume a constant $\phi_{\rm d}$ value of 0.77 of the maximum experimental kicking strength, $\phi_{\rm d,max}$. The effect of the spread in kicking strengths on the initial Shepelyansky diffusion rates is easily examined and also applies to the late-time energies. If $\rho(r)$ is the 2-dimensional cloud density as a function of radius r, and $\phi_{\rm d}(r)$ the distribution of kicking strengths, then we define the diffusion rate for a given $\phi_{\rm d,max}$ as [15]

$$\bar{D}(\phi_{\rm d,max}, T) = \int_0^\infty D(\phi_{\rm d}(r), T)\rho(r)2\pi r dr, \qquad (9)$$

where $D(\phi_{\rm d}(r), T)$ is given by Eq. (6). Calculating $\bar{D}(\phi_{\rm d,max}, T)$ for a broad kicking beam with $\sigma_{\rm cloud} << \sigma_{\rm beam}$, corresponding to constant $\phi_{\rm d}(r)$, reproduces the pronounced structure as seen in Fig. 1 and in the simulations. But calculating the diffusion rate with the 2:1 beam-to-cloud width ratio as used experimentally and with $\phi_{\rm d,max} = \phi_{\rm d}/0.77$, gives less accentuated diffusion resonance structure which is broader over the pulse period values. Fig. 3 displays these results for a few values of $\phi_{\rm d}$. Thus, a spread in $\phi_{\rm d}$ values creates an averaging effect which diminishes and broadens the resonance structure.

A spread in $\phi_{\rm d}$ values is also caused by atoms in different magnetic substates of the $F = 4$ level coupling to the higher energy states with different transition strengths, resulting in atoms in different substates experiencing different kicking strengths. The combination of this effect with that caused by the finite beam width can create a spread of $\phi_{\rm d}$ values which is as large as 20% of the mean $\phi_{\rm d}$ value. In order to account for this, we performed additional simulations in which the $\phi_{\rm d}$ value for each trajectory was chosen from a distribution based on the 2:1 beam-to-cloud width ratio for our system (assuming that each has a radial Gaussian profile). Also factored in were the relative coupling strengths of atoms in different magnetic substates for the experimental detunings $\delta = 315, 385, 485, 575, 655$ MHz for $\phi_{\rm d} = 3.3, 4.0, 5.0, 5.9, 6.6$ respectively (assuming an equal population of atoms in each substate). The results of these simulations are shown in the bottom row of Fig. 2. These additional simulations give much better agreement with the results, with the resonance structure being less pronounced. Also, the greater broadness of the overall structure in the results, particularly noticeable for $\phi_{\rm d} = 3.3$, is accounted for.

However, there is still some discrepancy in energy values between the experimental results and the additional simulations. For $\phi_{\rm d} = 5.9$ and 6.6 the measured energies are overall much lower than expected, while for all $\phi_{\rm d}$ they are much larger than in the simulations around the quantum resonance region of T = 58-68 μs. The first problem is accounted for by realising that in recording the momentum distributions, at some point signals at higher momenta fall below the noise level and therefore are effectively "lost in the noise". Hence, the measured total energy of the cloud is systematically lower than the true energy after kicking. For bigger $\phi_{\rm d}$, for which energies are higher in general, this problem is particularly pronounced as more atoms lie in the wings of the distribution. The discrepancy around the quantum resonance currently remains unexplained, but could be a systematic effect related to the larger pulse period values in this region. Continuing investigations will hopefully resolve this issue.

Overall, agreement between the experimental results and the additional simulations is very good, with clear structure evident and the amount of detail increasing with $\phi_{\rm d}$ as expected. For comparison, the energies for the classical system after 30 kicks were also computed by assuming that the diffusion rate for the first two kicks is $\phi_{\rm d}/4$, and for subsequent kicks is given by Eq. (7). They were averaged over the same spread in $\phi_{\rm d}$ values that was used in the additional quantum simulations and are shown in the bottom row of Fig. 2. Note that the energies are larger than the quantum simulations, as it would be expected, and for $\phi_{\rm d} = 5.9$ and 6.6 go off the scale, oscillating around $E' = 300$ and 560 respectively. With regards to their structure, the classical energies clearly exhibit very different behaviour from those measured in

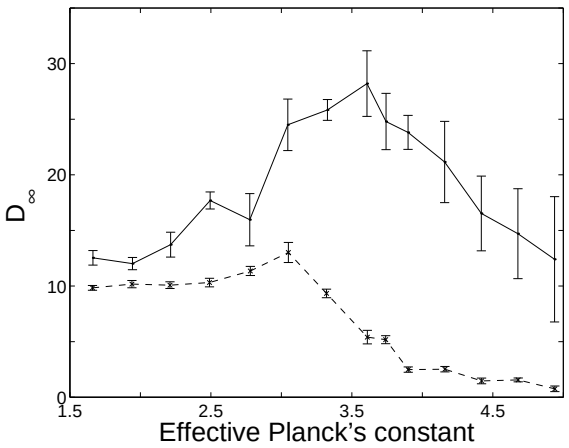

FIG. 4: Experimental results (solid line) and the corresponding quantum simulations averaged over the spread of κ values (dashed line) giving the late-time diffusion rate, D_∞, in scaled units for $\kappa = 11$, $\eta = 0.012$ and a maximum α of 0.015.

the quantum system, which confirms that the recorded resonance structure is a quantum effect.

B. Varying $\bar{k}$ while keeping κ constant

Keeping $\phi_{\rm d}$ constant and examining the energy after a certain number of kicks is the most straightforward experimental method of investigating diffusion resonances. However, for the kicked rotor it is not the most natural choice of experiment or units. It would be preferable to work with a constant κ rather than $\phi_{\rm d}$, for in the latter as we change the pulse period we effectively deal with a different kicked rotor system each time. For theoretical considerations it is more direct to keep κ constant, as well as η and α, and directly examine the diffusion rate in scaled units as a function of $\bar{k}$. In this way the structure in the quantum-to-classical transition for a single rotor system can be investigated directly.

We will now briefly look at a experimental realisation of such an investigation and the subsequent results. As was reported previously in Ref. [8], Shepelyansky's result also gives rise to resonance structure in the initial diffusion rates in scaled momentum units as the effective Planck's constant $\bar{k}$ is varied. The "locking in" effect causes the same structure to be observable in the late-time diffusion rate, D_∞, and it is this rate that we have also investigated experimentally.

The experimental method was quite similar to that for the previous results, but with some important differences. Firstly, to keep the theoretical parameters κ and η constant as $\bar{k}$ is varied requires a different kicking beam detuning, power and pulse length for each point on the curve. In finding a viable set of parameters, taking into account experimental limitations and theoretical considerations, one concession that had to be made was to vary the parameter $\alpha = \tau_p/T$ at higher $\bar{k}$. However, as α was reduced - which tends to increase diffusion rates - in a region where D_∞ is expected to decrease, no additional feature should appear. Reducing α as such stretched the upper $\bar{k}$ limit to 4.9. The first quantum resonance at $\bar{k} = 2\pi$ is therefore not seen in the results presented here. To estimate the late-time diffusion rate the energy, $E(N) = \langle \rho^2 \rangle/2$, of the cloud after 16 and 30 kicks was measured to give $D_\infty \approx (E(32) - E(16))/16$. As the momentum distributions in the measurement units of two-photon recoils were quite narrow a truncation of the wings of the measured distributions was possible. This further reduced the effect of noise in this high-momentum region on the measured energies. Simulations of Eq. (3) were performed as before, taking into account the spread in κ due to the finite kicking beam width and differing transition strengths for the various magnetic sublevels of the $F = 4$ level.

Fig. 4 displays the measured and simulated late-time diffusion rate as a function of $\bar{k}$ for $\kappa = 11$, $\eta = 0.012$ and a maximum α of 0.015, where α decreases from $\bar{k} = 3.7$ onwards to be finally 0.012 at $\bar{k} = 4.9$. Note that this is only a 20% decrease in the value of α, and, as mentioned above, cannot cause the decrease in diffusion rate seen in this area.

We see in the experimental results that a peak in the diffusion rate occurs as expected, but the quantitative agreement with the simulations is poor. The placement of the peak is somewhat to the right as compared to theoretical simulations and the measured diffusion rates are greater than expected, with those at higher $\bar{k}$ significantly larger than the simulations. We are currently performing further investigations, which will hopefully uncover the source of these problems and improve the agreement between the simulations and experimental results. Also note that the larger error bars for the diffusion rates at higher $\bar{k}$ are caused by the momentum distributions in the measurement units of two-photon recoils becoming narrower in these regions, thus making energy differences more difficult to resolve.

Nevertheless, a peak in the experimental results is evident; a clear observation of action-space diffusion resonances. The transition region between the quantum and classical regimes is indeed not as smooth as one would expect. It contains a diffusion peak separate from the quantum resonances as predicted by Shepelyansky's result.

VI. CONCLUSION

In conclusion, we have presented experimental and simulation results showing non-trivial behaviour in the late-time energy and diffusion rate as the pulse period/$\bar{k}$ is varied for the quantum kicked rotor. Very good qualitative agreement between the results and simulations can be seen. The relationship between the observed structure to Shepelyansky's scaling for the quantum correlations is evident. Furthermore, we note that the structure observ-

able in the late time energies confirms that in a system subject to environmental coupling a dependence of the late-time diffusion rate on the initial quantum diffusion rate exists.

Investigations are currently underway to discover the source of remaining discrepancies between the simulations and experimental results. We have also begun studies of similar diffusion resonances found in the quantum kicked rotor with the addition of amplitude noise on the kick strength and noise on the period between kicks.

This work was supported by the Royal Society of New Zealand Marsden Fund, grant UOA016.

[1] W. H. Zurek, Physics Today p. 36 (1991).
[2] H. Ammann, R. Gray, I. Shvarchuck, and N. Christensen, Phys. Rev. Lett. **80**, 4111 (1998).
[3] A. C. Doherty, K. M. D. Vant, G. H. Ball, N. Christensen, and R. Leonhardt, J. Opt. B: Quantum Semiclass. Opt. **2**, 695 (2000).
[4] B. G. Klappauf, W. H. Oskay, D. A. Steck, and M. G. Raizen, Phys. Rev. Lett. **81**, 1203 (1998).
[5] V. Milner, D. A. Steck, W. H. Oskay, and M. G. Raizen, Phys. Rev. E. **61**, 7223 (2000).
[6] D. A. Steck, V. Milner, W. H. Oskay, and M. G. Raizen, Phys. Rev. E. **62**, 3461 (2000).
[7] T. Bhattacharya, S. Habib, K. Jacobs, and K. Shizume, Phys. Rev. A. **65**, 032115 (2002).
[8] A. J. Daley, A. S. Parkins, R. Leonhardt, and S. M. Tan, Phys. Rev. E **65**, 035201 (2001).
[9] D. L. Shepelyansky, Physica **28D**, 103 (1987).
[10] B. G. Klappauf, W. H. Oskay, D. A. Steck, and M. G. Raizen, Phys. Rev. Lett. **81**, 4044 (1998).
[11] M. G. Raizen, Adv. At. Mol. Opt. Phys. **41**, 43 (1999).
[12] D. Cohen, Phys. Rev. A. **44**, 2292 (1991).
[13] H. Ammann, R. Gray, I. Shvarchuck, and N. Christensen, J. Opt. B: At. Mol. Opt. **31**, 2449 (1998).
[14] M. B. d'Arcy, R. M. Godun, M. K. Oberthaler, G. S. Summy, and K. Burnett, Phys. Rev. E **64**, 056233 (2001).
[15] M. P. Sadgrove, Master's thesis, University of Auckland (2002).